Novel EUV Mask Blank Defect Repair Developments

EUV Mask Blank Technology Transfer Program (LLNL and LBNL)

Stefan P. Hau-Riege, Anton Barty, and Paul Mirkarimi

Lawrence Livermore National Laboratory
L-395, PO Box 808, Livermore, CA 94550

March 31, 2003

Submitted to
Phil Seidel
International SEMATECH
2706 Montopolis Drive
Austin, TX, 78741

Contents

This work was performed under the auspices of the U.S. Department of Energy by University of California, Lawrence Livermore National Laboratory under Contract W-7405-Eng-48. This project is supported by International SEMATECH under Project Lith 233.

1. Executive Summary

The development of defect-free reticle blanks is an important challenge facing the commercialization of extreme ultraviolet lithography (EUVL). The basis of EUVL reticles are mask blanks consisting of a substrate and a reflective Mo/Si multilayer. Defects on the substrate or defects introduced during multilayer deposition can result in critical phase and amplitude defects. Amplitude- or phase-defect repair techniques are being developed with the goal to repair many of these defects. In this report, we discuss progress in two areas of defect repair:

1. We discuss the effect of the residual reflectance variation over the repair zone after amplitude-defect repair on the process window. This allows the determination of the maximum tolerable residual damage induced by amplitude defect repair.
2. We further performed a quantitative assessment of the yield improvement due to defect repair. We found that amplitude- and phase-defect repair have the potential to *significantly* improve mask blank yield. Our calculations further show that yield can be maximized by *increasing* the number of Mo/Si bilayers.

2. Scope and Context of the Report

This report is the first milestone report for the EUV mask blank defect repair developments project conducted at the VNL, which forms sub-section 4 of the Q1 2003 ISMT mask blank technology transfer program at the VNL. Specifically this report addresses deliverables 3.4.1.1, 3.4.1.2, and 3.4.2.1.

The overall goal of this project is to provide additional learning on both phase and amplitude repair strategies. Accordingly, VNL has conducted the project activity on the development of amplitude defect repair (through use of ion beam or nano-machining or new techniques), development of phase defect repair (through use of e-beam or nano-machining or new techniques), and the future demonstration of repair effects through imaging of repaired mask blanks on either the MET or LBNL AIMS beamline. In particular this report addresses the development of a realistic model for the acceptable reflectance variation over the amplitude repair zone, and the development of a comprehensive model for the impact of defect repair on mask blank yield.

After a brief introduction to defect repair, we discuss a model for the effect of the reflectance variation over the amplitude repair zone on CD variation, which addresses deliverable 3.4.1.1. We will then discuss a model for the yield improvement due to amplitude and phase defect repair. This addresses deliverables 3.4.1.2 and 3.4.2.1.

3. Background

The basis for EUVL reticles are mask blanks that consist of a ultra-low-expansion substrate and a multilayer stack of alternating layers of Mo and Si to reflect light around 13.4nm. A major yield limiter for mask blanks are defects that introduce errors in the printed image. Several defect reduction schemes such as optimization of the reflective multilayer deposition process have been suggested [1], but it is questionable if these techniques alone will be sufficient to meet the stringent requirements for EUVL reticle production [2]. Alternatively, it has been suggested that mask blank yield can be improved by repairing defective mask blanks [3].

Defects near the bottom of the multilayer stack tend to primarily modify the phase of the reflected light and are named *phase defects*, whereas defects located toward the top of the multilayer stack tend to attenuate the amplitude of the reflected light, and are called *amplitude defects*. Depending on the nature of the defect, different defect repair techniques can be used. The *amplitude-defect repair* technique removes the particle along with the damaged region of the multilayer using a focused ion beam, leaving behind a shallow crater in the multilayer. This crater needs to be capped in order to prevent oxidation, because oxidized Mo leads to a severe drop in the reflectance. The amplitude-defect repair technique is primarily aimed at repairing amplitude defects near the surface of the multilayer. The *phase-defect repair* technique uses a high-resolution electron beam to heat the multilayer locally to activate silicide formation. This results in a local contraction of the multilayer structure [3], which counteracts the deformation of the multilayer near a defect during multilayer growth. Phase-defect repair is primarily aimed at repairing defects nucleated by particles near the bottom of the multilayer stack.

A major challenge for amplitude-defect repair is the variation of the reflectance over the repair zone. We will report on the effect of the reflectance variation on changes in linewidth in the printed image, and its effect on the process window. In the second part of this report, we will discuss the effect of amplitude and phase defect repair on yield improvement of mask blanks using Monte-Carlo simulations.

4. A realistic model for determining the acceptable reflectance loss in repaired region based upon the allowable CD variation in the printed image (Deliverable 3.4.1.1).

Introduction

Even with a capping layer, amplitude-defect repair leads to a residual variation of the reflectance over the repair zone [4]. This variation of the reflectance leads to a variation of the linewidth in the printed image, where the smallest features of critical dimensions (CD) are affected most.

We determined the effect of the reflectance variation due to amplitude-defect repair on CD by computing the change of the process window in the presence of a repair zone. The process window defines the ranges of dose and focus that result in CD's within allowed limits. We calculate the process windows for the cases of (i) no defects and therefore without a repair zone, (ii) in the presence of unrepaired amplitude defects, and (iii) with a repair zone. Comparing the process windows of case (ii) and (iii) demonstrates the benefit of the amplitude repair technique. The process window obtained for case (iii) needs to be inspected to determine if the reflectance variation over the crater is acceptable.

We would like to point out that during the course of this work it became apparent to us that a simple model for determining the acceptable reflectance loss in the repaired region based upon the allowable CD variation in the printed image is not appropriate. In a holistic view of the lithographic process, the combined effects of reflectance loss and dose and focus need to be considered. Instead, we opted to calculate how the process window shrinks due to a certain reflectance loss. It then needs to be determined if this smaller process window is still acceptable or not. This path is somewhat more complicated than what was originally proposed, but avoids oversimplification.

Theory

To calculate the process window, we compute the partially-coherent image of an infinite set of lines and spaces. We assume that the illumination profile is constant (top-hat shaped), and that the pupil is aberration-free. [In future work we will need to consider the effect of aberrations.] Assuming a threshold resist, we then determine the CD of the printed image. This process is repeated for several doses and focuses, which results in the process window as a function

of numerical aperture, wavelength, coherence factor for top-hat illumination, threshold of photo resist in fraction of the illumination, positivity of the photo resist, linewidth and pitch of the lines on the mask, range of dose and focus, and range of allowed CD variations.

We assume that the crater profile of the amplitude repair zone does not scatter light outside of the camera pupil, and that the phase profile across the repaired region through focus is not printable. In Appendix A we show that this is the case for a large crater with gently sloping sides [5]. In Appendix B it is demonstrated that for a typical amplitude repair zone, the image placement error is negligible, and that the typical crater depth is much smaller than the depth of focus of the mask [5].

A change in reflectance over the repair zone is, from a computational point of view, equivalent to a change in dose. So we recalculate the process windows with the minimum negative change in reflectance, shifting the process window to larger doses, and with maximum positive change in reflectance, shifting the process window to smaller doses. The overlap of both windows gives the ranges of dose and focus that result in CD's within allowed limits on virgin multilayers as well as on repaired multilayers.

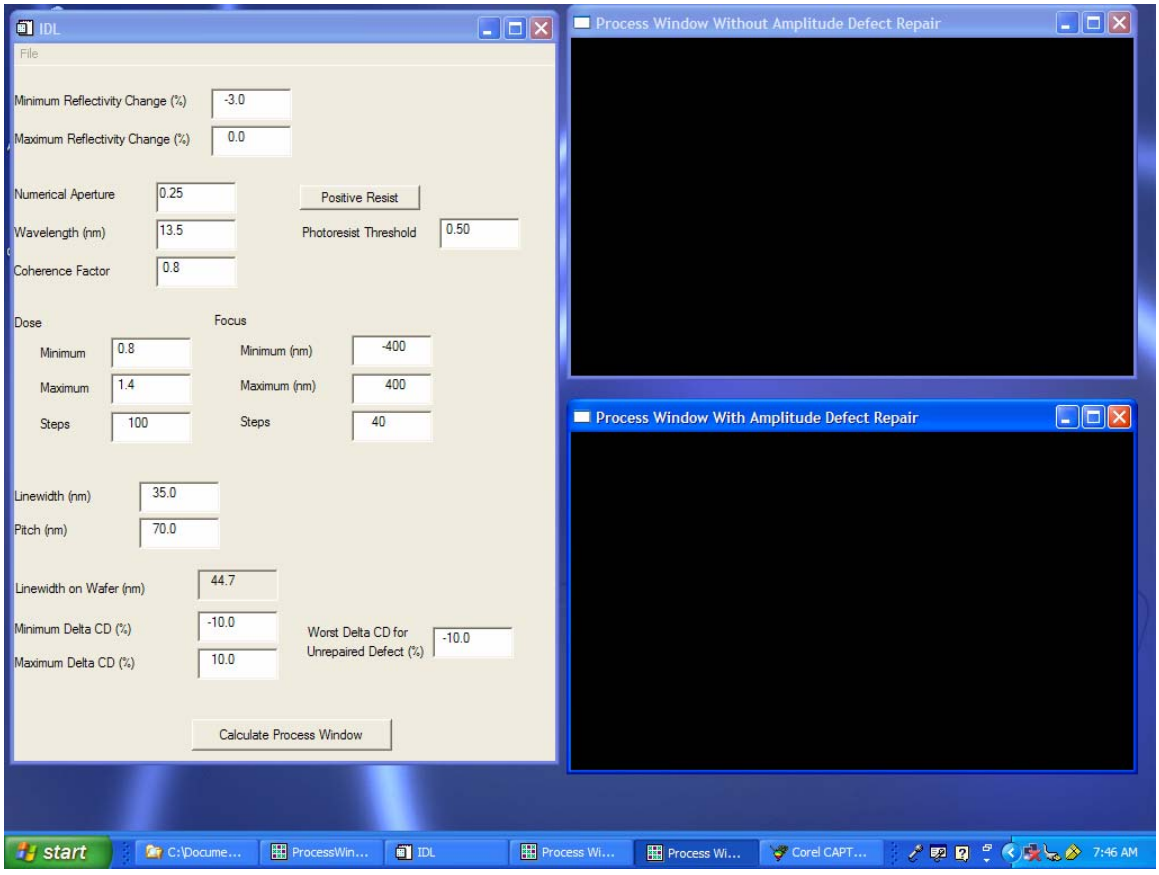

Figure 1: Screenshot of program to calculate process window, *CraterPrinting*.

Description of Computer Code

The computer code to calculate the process windows requires IDL Version 5.6. IDL is an interactive data language for data analysis and visualization. It can be downloaded from http://www.rsinc.com, and a license is available from Research Systems Inc., 4990 Pearl East Circle, Boulder 80301. We assume IDL is installed on the computer system to run the code.

To start the program with its graphical user interface, double-click on SEMATECH\ProcessWindow\ProcessWindow.prj. After IDL starts up, click on "Compile Project Files" to compile the whole program, and enter *CraterPrinting* in the command line. The program will start and present a screen as shown in Figure 1. The left window is the input window for the simulation parameters, and the right two windows are the output windows for the simulation results.

Amplitude Repair Zone	
	Minimum reflectivity change
	Maximum reflectivity change
Optics	
	Numerical aperture
	EUV Wavelength
	Coherence Factor
Photoresist	
	Threshold
	Positivity
Process Window	
	Dose range
	Focus range
Pattern	
	Linewidth
	Pitch
CD Control	
	Minimum allowed CD change
	Maximum allowed CD change
	Worst-case CD change for unrepaired defect

Table I: Input parameter for the program code to calculate the process window.

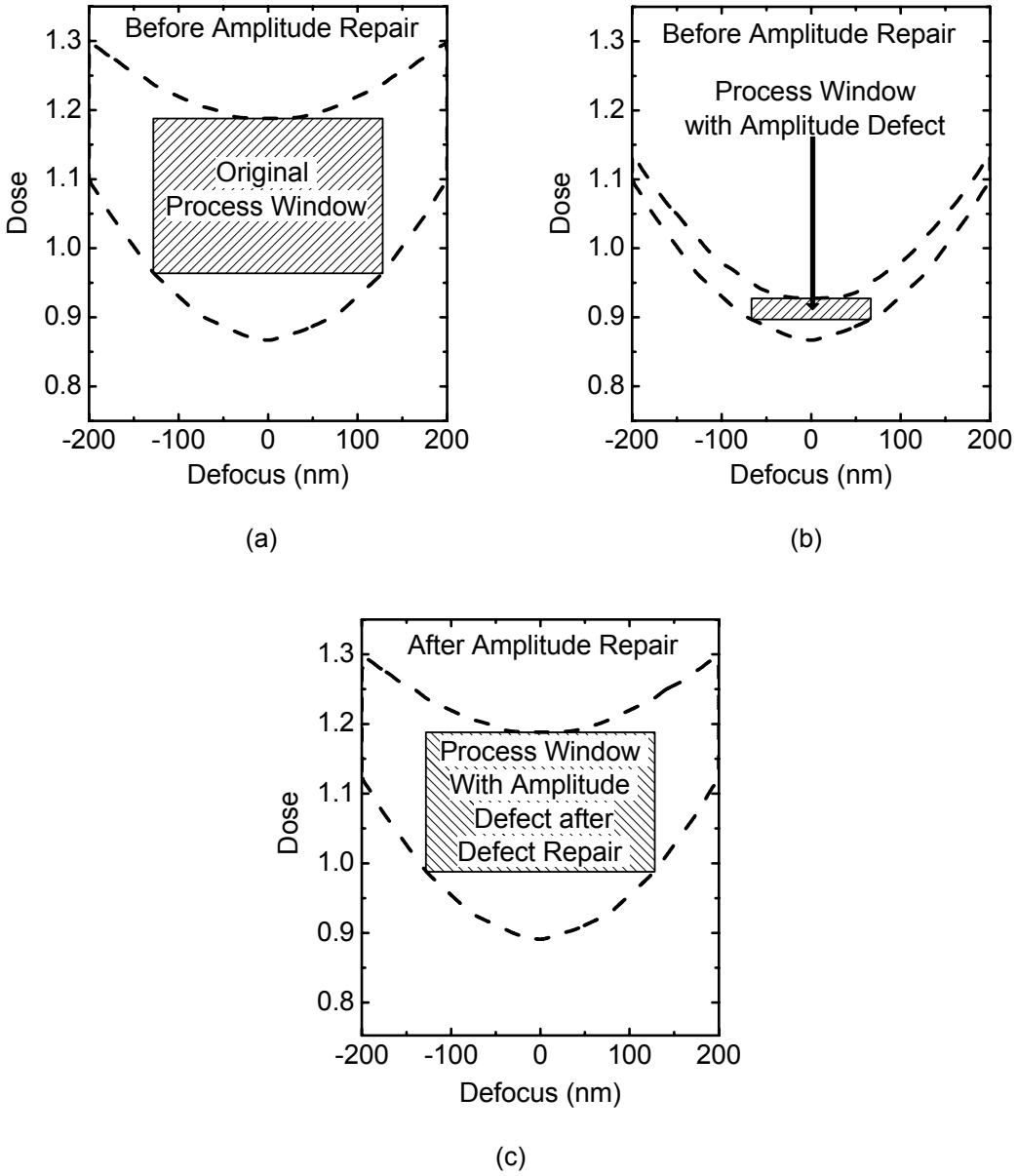

Figure 2: (a) Dose-defocus process window without defects. (b) Process window with a defect that leads to a relative CD variation of +15%. For a relative CD change that is greater than 20% the process window diminishes. (c) Restored process window after amplitude defect repair.

We first discuss the input parameters, which are listed in Table I. Our goal was to make as many parameters as possible accessible to the user to ensure the universal applicability of the program. The maximum and minimum reflectance changes over the repair zone determine the maximum and minimum CD variations. The reflectance variations are typically determined experimentally, and entered near the top of the input window. Various parameters describing the lithography system, such as numerical aperture,

wavelength, coherence factor, resist positivity, and resist threshold can be modified. The range of dose and focus needs to be entered, along with the number of steps for the discretization of the process window. A larger number of steps increases the accuracy of the simulation. The width and pitch of the line array on the mask can be entered, and the program automatically calculates the linewidth on the wafer. The process window is determined by the maximum and minimum acceptable CD variation, and the user needs to enter the worst-case CD variation for an unrepaired defect to allow the comparison of the process window with and without repair.

The simulation is started by clicking on “Calculate Process Window”. The window on the top right shows the process window without amplitude-defect repair. The dotted line encloses the process window in case no defects are present, and the solid line encloses the process window in the case a defect is present. The rectangles are rectangles of maximum area within the process window. The window on the bottom right shows the process window after amplitude repair. The solid line shows the process window corrected for the reflectance variation over the repair zone. For comparison, we show the process window in case no defects are present again (dotted line). Note that in Figure 2 we reformatted the output of the simulation.

Initial Modeling Results

We determined the process window for arrays of 35nm-wide lines spaced 35nm apart, assuming a threshold resist with a threshold of 50%, a completely opaque mask, an imaging system with NA=0.25, and a partial coherence of 0.8. The process window was determined by allowing a maximum relative CD variation of $|\Delta CD/CD| \leq 10\%$.

Figure 2 (a) shows the process window without amplitude repair. An amplitude defect effectively shrinks the process window, as shown in Figure 2 (b). For an amplitude defect that leads to a CD increase of larger than 20%, the process window diminishes. Amplitude-defect repair restores part of the process window, as shown in Figure 2 (c). These results demonstrate that even though amplitude defects can nearly or completely diminish the process window, as shown in Figure 2 (b), amplitude defect repair can nearly completely restore this process window, as shown in Figure 2 (c).

5. Realistic, comprehensive model for the impact of amplitude and phase defect repair on the mask cost-of-ownership (Deliverable 3.4.1.2 and 3.4.2.1)

Introduction

We decided to combine both deliverables and develop a single model that allows the determination of the benefit of amplitude-defect repair alone, phase-defect repair alone, and in addition the benefit of both repair techniques combined. For maximum flexibility, we opted to calculate the yield improvement due to the repair techniques as a measure for the impact of defect repair on the mask cost.

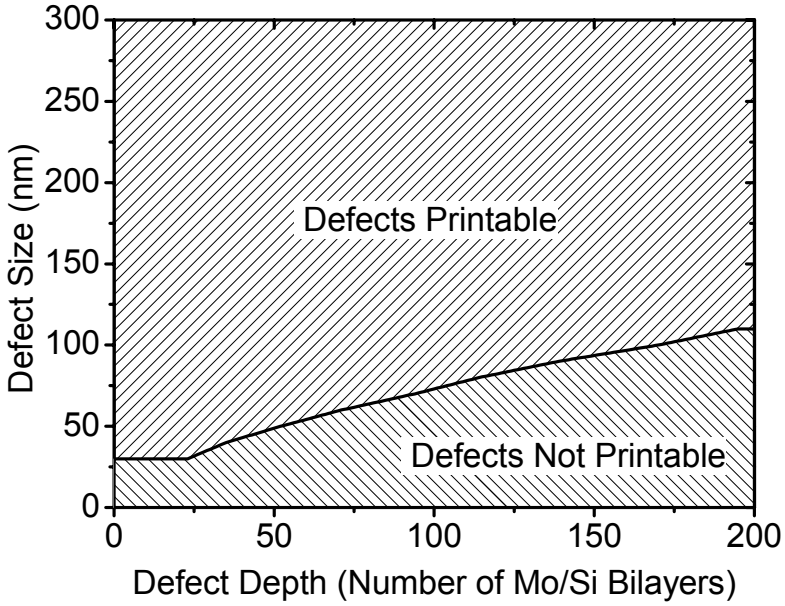

Figure 3: Printability of defects as a function of defect size and depth in the multilayer.

Theory

Both defect printability and defect repairability depend on the defect size and the vertical position of the defect in the multilayer stack. The defect size is taken as the maximum defect diameter, and the vertical position is in units of the number bilayers from the top surface. It is computationally very intensive to calculate the exact dependence of defect printability and phase-defect repairability on defect size and vertical position. For the printability, rigorous electromagnetic modeling

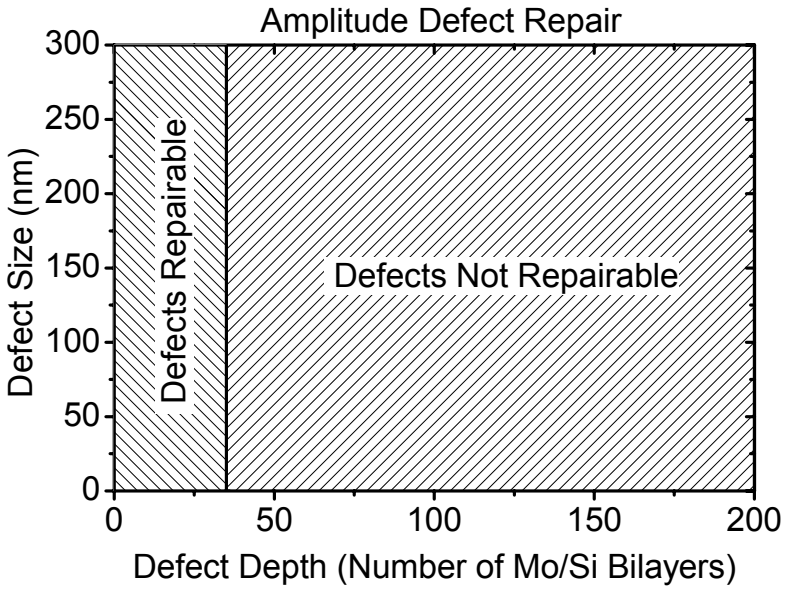

(a)

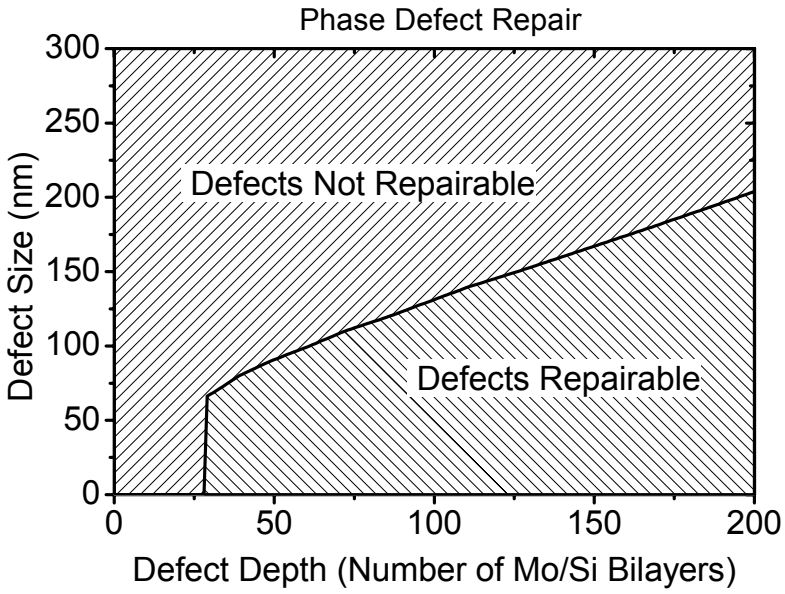

(b)

Figure 4: Phase spaces of repairable and unrepairable defects for (a) amplitude defect repair and (b) phase defect repair. For amplitude defect repair, the space of repairable defects is smaller if the total number of bilayers is smaller than 70 since a certain number of bilayers must remain to ensure a minimum reflectivity in the repair zone.

is necessary. For the phase-defect repairability, in addition the interaction of the multilayer with the electron beam has to be taken into account, and the electron beam parameters need to be optimized for each defect size and location. Further, the results depend on the details of the multilayer deposition process. Instead of performing these rigorous calculations, we opted for a grosser estimate instead, since we only want to point out general dependencies rather than characterizing a specific fabrication process. For the dependence of printability on defect size and location, we assumed that any defect smaller than 30nm on the mask does not lithographically print. This is consistent with a maximum CD variation of 20% for the 45nm technology node. Further, we calculated the surface bump height for defects of different sizes and locations assuming an ion-assisted ion-beam deposition process, as described in reference [6], and considered a defect unprintable if the bump height at the surface is less than ~1nm. The resulting curve is shown in Figure 3. Similarly, we considered the defect phase-repairable, if there are at least 30 Mo/Si bilayers on top of the defect and if the bump height is less than 4nm [3]. The resulting curve is shown in Figure 4 (a).

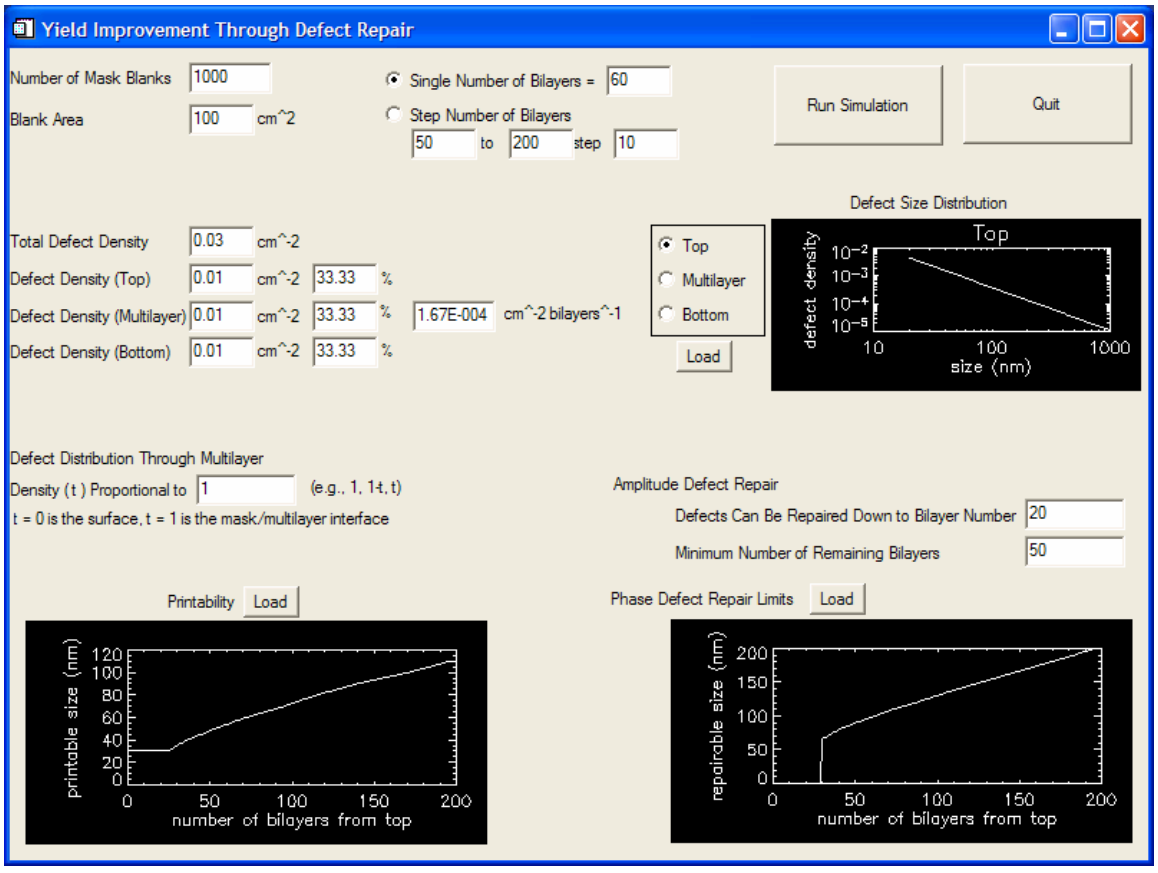

Figure 5: Screen shot of program to calculate yield improvement due to repair, *RepairYield.*

The dependence of the repairability of amplitude defects on defect size and location can be estimated somewhat more precisely. With amplitude-defect repair, defects of any size smaller than the repair zone, which is typically several

micrometer, can theoretically be repaired. All defects near the surface of the multilayer can be repaired, provided that at least 35 Mo/Si bilayers remain underneath the repair zone to maintain a certain minimum reflectance, and provided that no more than 35 Mo/Si bilayers are removed to constrain the image placement error to less than 6nm [5]. The resulting dependence is shown in Figure 4 (b).

We then performed Monte-Carlo simulations to obtain the distribution of printable defects on mask blanks with and without amplitude- and/or phase-defect repair.

Description of Computer Code

The computer code to calculate the process windows requires IDL Version 5.6. IDL is an interactive data language for data analysis and visualization. It can be downloaded from http://www.rsinc.com, and a license is available from Research Systems Inc., 4990 Pearl East Circle, Boulder 80301. We assume IDL is installed on the computer system to run the code.

To start the program with its graphical user interface, double-click on SEMATECH\RepairYield\RepairYield.prj. After IDL starts up, click on “Compile Project Files” to compile the whole program. Note that this has to be done two times to resolve forward references in the program. Then enter *RepairYield* in the command line. The program will start and present open the input window as shown in Figure 5.

The simulation can be run in two modes: (i) The calculations are done for a fixed multilayer thickness. The number of Mo/Si bilayers needs to be entered. (ii) The program steps through a range of multilayer thicknesses. In this case, the maximum and minimum number of bilayers, as well as the step size need to be entered. The defect density in the multilayer film is calculated from the defect density per number of bilayers. In both cases, the simulations are performed for a certain number of mask blanks. It turns out that the results converge if 50,000 mask blanks or more are used.

Various distributions of defect sizes and locations can be used in the simulations. The defects are categorized in three groups. The first group consists of the defects that are located on top of the Mo/Si multilayer (“Top”). The second group consists of the defects that are distributed through the bulk of the multilayer film (“Multilayer”). The third and final group consists of the defects that are located at the bottom of the multilayer stack (“Bottom”). For each group, a separate defect density and defect size distribution can be entered. Further, spatial distribution of defects through the thickness of the multilayer can be entered. By default, this is set to 1, which means that the defect density is

constant through the multilayer. The size and spatial distributions are normalized to match the selected defect density.

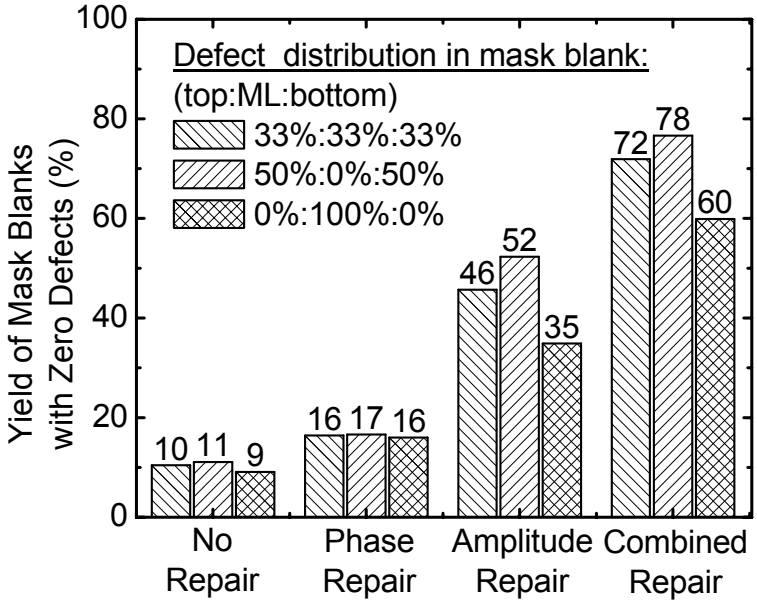

(a)

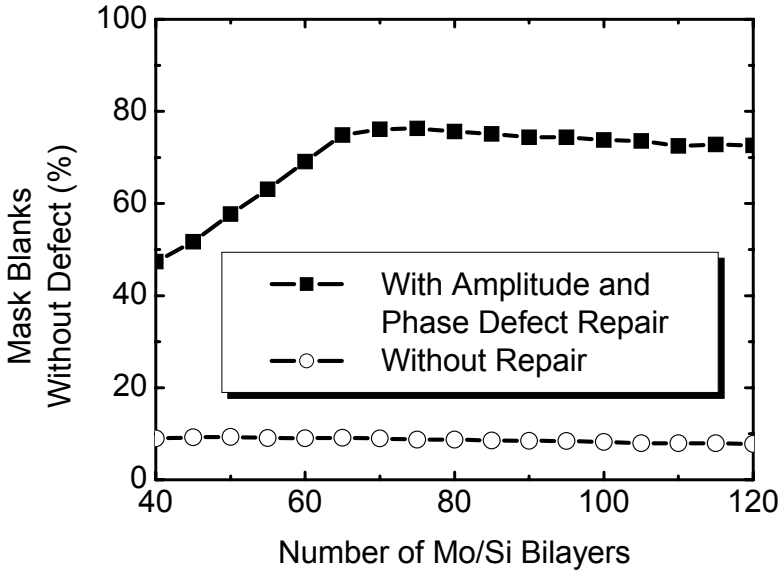

(b)

Figure 6: (a) Yield of mask blanks with zero defects without repair, with phase repair only, with amplitude repair only, and with amplitude and phase defect repair, respectively. We performed the calculations for three different distributions of defects in the mask blank. (b) Yield of mask blanks with zero defects as a function of number of Mo/Si bilayers with and without defect repair.

The user needs to provide data for the maximum defect size that is lithographically printable as a function of position in the multilayer stack. As discussed in the theory section, for amplitude defect repair the minimum number of remaining bilayers and the maximum crater depth need to be selected. For phase defect repair, the user needs to provide the maximum defect size as a function of depth that can be repaired.

The simulations are started by clicking on “Run Simulation”. When the calculations are done, an output window is opened with the simulation results. The data can be saved into an ASCII file by pressing “S”, and the window contents can be printed into a postscript file by pressing “P”. “Q” will close the window. If only one multilayer thickness is simulated, the output window will show five graphs of the fraction of mask blanks as a function of number of defects on a cumulative plot. If multiple multilayer thicknesses are simulated, the output window shows also five graphs. From left to right and top to bottom these are (i) fraction of mask blanks containing 0,1,or 2 defects on the mask, (ii) fraction of mask blanks containing 0,1,or 2 *printable* defects on the mask, (iii) fraction of mask blanks containing 0,1,or 2 *printable* defects on the mask *after phase-defect repair*, (iv) fraction of mask blanks containing 0,1,or 2 *printable* defects on the mask *after amplitude-defect repair*, and (v) fraction of mask blanks containing 0,1,or 2 *printable* defects on the mask *after both phase- and amplitude-defect repair*.

Initial Modeling Results

We performed Monte-Carlo simulations to obtain the mask blank yield, where we define yield as the fraction of mask blanks without any printable defects [4]. We assumed that the defect density is proportional to $d^{-1.5}$, where d is the defect diameter [7], and that the mask blanks have a quality area of $(14.2\text{cm})^2$ [8]. For each set of simulation parameters, we performed calculations for 50,000 mask blanks.

Figure 6 (a) shows the yield of mask blanks as a function of defect repair treatment, as obtained by Monte-Carlo simulations, for a multilayer coating of 60 Mo/Si bilayers. The calculations were performed for three different distributions of the defects through the mask blank: In the first set of simulations, we assumed that 1/3 of the defects are located at the top surface of the multilayer, and 1/3 of the defects are located at the bottom surface of the multilayer. The remaining 1/3 of the defects are distributed uniformly throughout the bulk of the multilayer. In the second set of simulations, we assumed that the bulk of the multilayer is defect-free, and that 1/2 of the multilayer are present on the top and bottom multilayer surface, respectively. In the third set of simulations, we assumed that all the defects are uniformly distributed through the multilayer stack. In all three sets of simulations we assumed a total density of defects

larger than 20nm of 0.03/cm^2. [We chose a minimum defect size of 20nm to be consistent with the mask blank SEMI standard P38.] Figure 6 (b) shows the yield of mask blanks with and without repair as a function of number of Mo/Si bilayers in the multilayer. We assumed that the density of defects located at the top and bottom surface of the multilayer was 0.01/cm^2 each, and that the remaining defects were homogenously distributed through the multilayer stack, with a defect density of 2x10^{-4}/cm^2 per Mo/Si bilayer.

The results of our Monte-Carlo simulations of the yield improvement due to defect repair, as shown in Figure 6 (a), clearly demonstrate that both amplitude and phase defect repair have the potential of significantly reducing the number of yield-limiting defects. We found that this conclusion holds true even for very different distributions of defects through the mask blank. The simulations also show that the yield improvement due to the combined application of amplitude- and phase-defect repair exceeds the simple sum of the yield improvements of amplitude- and phase-defect repair alone. This synergetic effect is due to the fact that amplitude-defect repair is aimed at repairing defects located toward the top surface of the multilayer, whereas phase-defect repair is aimed at repairing defects located toward the bottom of the multilayer stack, and that both techniques applied together potentially address defects though the full multilayer stack.

As shown in Figure 6 (b), defect repair is predicted to be beneficial for mask blank yield regardless of the number of Mo/Si bilayers in the multilayer. In these simulations we assumed that 1/3 of the defects are located at the top surface of the multilayer, so that in the case no repair techniques are used, the yield decreases only slightly with increasing number of bilayers, since top-surface defects dominate. For 40 to 70 bilayers, the yield of mask blanks after repair increases with increasing number of bilayers since amplitude-defect repair is able to repair defects that are located deeper into the multilayer. The additional number of defects due to the deposition of more bilayers is small. However, restrictions on image displacement limit the maximum number of bilayers that can be removed during amplitude-defect repair, and amplitude-defect repair does not help if the number of bilayers is increased further. Increasing the number of bilayers beyond 70 may then lead to a slow degradation of yield since the deposition of additional bilayers adds more defects. In summary, there is an optimum multilayer thickness that leads to a maximum yield improvement using amplitude- and phase-defect repair.

6. References

[1] P.B. Mirkarimi, E.A. Spiller, D.G. Stearns, V. Sperry, and S.L. Baker, *An ion-assisted Mo-Si deposition process for planarizing reticle substrates for extreme ultraviolet lithography*, Quant. Elect. Lett. **37**, 1514 (2001).

[2] EUV Mask and Chuck Standard SEMI P38-1102, published by International SEMATECH (2002).
[3] P.B. Mirkarimi, D.G. Stearns, S.L. Baker, J.W. Elmer, D.W. Sweeney, and E.M. Gullikson, *Method for repairing Mo/Si multilayer thin film phase defects in reticles for extreme ultraviolet lithography*, J. Appl. Phys. **91**, 81 (2002).
[4] S.P. Hau-Riege, A. Barty, H. Chapman, P.B. Mirkarimi, D.G. Stearns, D. Sweeney, M. Clift, and E. Gullikson, *Defect repair for extreme ultraviolet lithography (EUVL) mask blanks,* Proc. SPIE **5037-43**, (2003).
[5] A. Barty, S.P. Hau-Riege, H. Chapman, P.B. Mirkarimi, D.G. Stearns, D. Sweeney, M. Clift, and E. Gullikson, *A method for repairing amplitude defects in multilayer-coated EUV mask blanks*, to be submitted.
[6] D.G. Stearns, P.B. Mirkarimi, and E.Spiller, *Localized defects in EUV multilayer coatings*, submitted for publication.
[7] S.D. Hector, P.A. Kearney, C. Montcalm, J.A. Folta, C.C. Walton, W.M. Tong, J.S. Taylor, P.-Y. Yan, and C. Gwyn, *Predictive model of the cost of extreme ultraviolet lithography masks*, Proc. SPIE **4186**, 733 (2001).
[8] S.D. Hector, *EUVL Masks: Requirements and Potential Solutions*, Proc. SPIE **4688**, 134 (2002).
[9] M.R.Teague, *Image formation in terms of the transport equation,* J. Opt. Soc. Am. **A11**. 2019 (1985).

Appendix A: Controlling phase errors in the amplitude repair zone

Milling away layers of the multilayer stack will introduce a phase shift into the reflected field, and it is therefore essential that the crater profile be carefully controlled so as to minimize printability of the repaired region in a lithographic tool. Multilayer reflection occurs throughout the multilayer bulk rather than from the surface, so when layers are removed by milling the phase of the reflected field does not simply follow the surface profile. Milling removes layers from the multilayer stack without altering their relative position; the layered structure of a multilayer mirror forces all waves to be in phase with respect to each other within the multilayer itself, thus after milling the only contribution to phase error occurs from the refractive index difference between the vacuum inside the crater and the multilayer bulk. The optical path difference (OPD) for light reflected from a Gaussian-shaped crater is therefore of the form

$$p(\vec{r}) = 2(n-1)h\exp\left(-\frac{r^2}{w^2}\right),$$

where n is the average refractive index of the multilayer, h is the maximum depth of the crater, and ω is the 1/e radius of the crater on the mask. The refractive index for a typical Mo/Si coating operating at an EUV wavelength of 13.5 nm is n

= 0.97. That is to say that the refractive index of the multilayer is very nearly the same as for vacuum, thus the phase shift for a given crater depth is just 0.03 times the profile of the crater itself.

Assuming that the crater profile is gentle enough that light is not scattered outside of the camera pupil the dominant effect of the crater phase structure within the process-window of the lithographic tool is due printability of the phase profile through focus, and it can be shown using arguments based on the transport of intensity equation [9] that the maximum contrast C_{max} within the process window of a lithographic tool is proportional to the slope of the wall of the crater and is given by

$$C_{max} = 1.45\frac{(1-n)N}{n(w/\delta)^2}.$$

Here δ is the spatial resolution of the lithographic tool facing the mask, and N is the number of bilayers removed, and we see that craters with gently sloping sides will not print as easily as craters with steep sides. For the removal of 20 bilayers from a Mo/Si multilayer mask we have $C_{min}=0.89\delta^2/\omega^2$, and to ensure that the contrast induced by the repair is less than 1% we must have $\omega>9.45\delta$. In practical terms this means that for a 0.25NA 4x stepper system operating at 13.5nm we need 20 bilayer (130nm) deep repair craters to be 4μm or more in diameter to ensure that the repaired region does not manifest itself as a phase defect in the printed image.

This appendix is going to be published in reference [5].

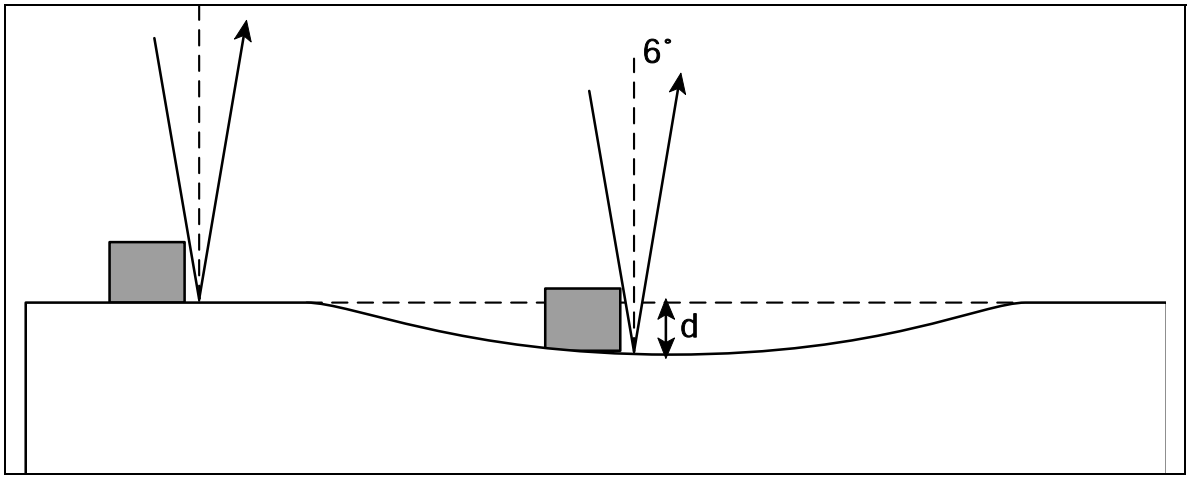

Figure B1: Image placement error caused when the pattern is placed within the crater.

Appendix B: Image placement error and depth of focus for amplitude defect repair

The absorber pattern in the repaired region will be at a different depth with respect to unrepaired regions of the mask, and this will cause a small amount of image placement error. The mask is illuminated by EUV light at an angle of 6° to the normal as illustrated in Figure B1, thus placing absorber features at different depths leads to some image placement error in the printed image. The magnitude of the image placememt error δx in the wafer plane can be determined from the geometric image shift and is given by

$$\delta x = M d \tan\theta,$$

where d is the crater depth, θ is the angle of illumination and M is the magnification of the projection optics. For a typical 0.25NA EUV projection optics we expect the angle of incidence to be approximately 6° ($\theta \approx 6^{o}$), and the reduction ratio to be a factor of 4 (M=0.25). The image placement errors calculated for absorber features positioned within the crater at different depths are listed in Table B1.

Depth of repair site (Number of bi-layers)	Depth of repair site (d, nm)	Worst-case image placement error $(\delta x, nm)$
2	13.8 nm	0.36nm
5	35 nm	0.9nm
10	69 nm	1.8nm
15	104nm	2.7nm
20	138nm	3.6nm
40	276nm	7.2nm

Table B1: Image placement errors

Inspection of Table B1 shows that the image placement error caused by the absorber being at a different depth within the repair site is comfortably within the allowed overlay budget of 15nm allowed at the 45nm technology node. [Note that the repair site is only an isolated region on the mask.] This is the image placement error at the worst place in the repair site, which itself is only microns in size, thus the added contribution to the overall overlay budget is both small in magnitude and occurs only in a small micron-sized region of the entire mask.

Note also that the anticipated depth of the repair region is well within the depth of focus of the projection optics. The depth of focus of an optical system is approximately

$$\mathrm{DOF} \approx \pm \frac{\lambda}{2(\mathrm{NA})^2}.$$

Thus for a typical 0.25NA, 4x reduction projection system the NA facing the mask will be 0.0625NA, giving a depth of focus at the mask of approximately ±1.7μm. This is much greater than the anticipated depth of the repair region, thus we do not anticipate any detrimental effects due to additional defocus caused by the absorber layer being placed at a different depth within the repair region, which itself is only a small micron-sized region of the entire mask.

This appendix is going to be published in reference [5].